

Chaotic dynamics of a frequency-modulated microwave oscillator with time-delayed feedback

Hien Dao,^{1,2,a)} John C. Rodgers,¹ and Thomas E. Murphy^{1,3}

¹*Institute for Research in Electronics and Applied Physics, University of Maryland, College Park, Maryland 20742, USA*

²*Chemical Physics Program, University of Maryland, College Park, Maryland 20742, USA*

³*Department of Electrical and Computer Engineering, University of Maryland, College Park, Maryland 20742, USA*

(Received 26 September 2012; accepted 4 December 2012; published online 4 January 2013)

We present a chaotic frequency-modulated microwave source that is governed by a simple, first-order nonlinear delay differential equation. When a sinusoidal nonlinearity is incorporated, the dynamical behaviors range from fixed-point to periodic to chaotic, depending on the feedback strength. When the sinusoidal nonlinearity is replaced by a binary nonlinearity, the system exhibits a complex periodic attractor with no fixed-point solution. © 2013 American Institute of Physics. [<http://dx.doi.org/10.1063/1.4772970>]

Time-delayed feedback systems are especially interesting because of the rich variety of dynamical behaviors that they can support. While ordinary differential equations must be of at least third-order to produce chaos, even a simple first-order nonlinear delay differential equation can produce higher-dimensional chaotic dynamics. Although there are many classic electronic circuits that produce chaotic behavior, microwave sources of chaos are especially relevant in communication and sensing applications where the signal must be transmitted between locations. Such applications invariably involve time-delays associated with the signal propagation. Here, we describe a new way to generate chaotic frequency-modulated microwave signals by using time-delayed feedback, and we explore the dynamical characteristics and route to chaos as the feedback strength or time delay is varied. We further introduce, implement, and analyze a new type of Boolean time-delayed feedback system that shows complex periodic orbits and fractal characteristics in its bifurcation behavior.

I. INTRODUCTION

After decades of research, chaos remains a fast-growing and exciting area in science and engineering. The evolution of the state of a chaotic system is deterministic, yet impossible to predict—a property that distinguishes chaos from randomness. Chaotic phenomena are observed in a wide variety of fields including electronics, mechanics, chemistry, biology, and acoustics. The complex and noise-like characteristics of chaotic signals could have advantages in a variety of practical applications. Chaotic signals have been proposed to reduce interference and cross-talk in diverse contexts, including wireless networks, sonar networks, fiber-optic links, and electric power systems.^{1–4} Chaotic modulation methods have been used to encrypt or mask information in

communication systems.^{5–7} The unpredictability of chaotic signals has been exploited for high-speed random number generation.^{8–12} Chaotic signals often exhibit a wide spectral bandwidth and a short correlation time, which are useful for increasing the precision of range and velocity detection in radar, lidar, and sonar systems.^{13–16}

Because many communication and ranging systems operate at microwave frequencies, a chaotic signal generator in this regime is of considerable interest. Although there are many classical electrical circuits that can produce broadband chaotic waveforms, it is often difficult to scale these systems to the microwave regime because in high-speed systems, the time delay associated with signal propagation is often non-negligible in comparison to the dynamical timescales. Chaotic generators that expressly rely on time-delayed feedback can take advantage of these unavoidable signal propagation delays.

One architecture that can be adapted to producing high-speed chaos is a nonlinear time-delayed feedback loop¹⁷ composed of a nonlinear circuit with time-delayed feedback through a band-limiting filter. The dynamical behavior of such a loop can be mathematically described by nonlinear delay differential equations. Recent works show that chaos can be generated with this architecture using a combination of optical and electronic components.^{18–20} The chaotic signals generated by these systems are examples of *amplitude chaos*, i.e., a signal with an irregular time-varying amplitude. However, for some applications in communication, it is preferable to use *phase chaos* in which the chaotic RF signal has a constant amplitude and a chaotic phase or frequency.²¹

In this paper, we introduce a chaotic signal generator that utilizes a time-delayed feedback loop architecture and operates in the microwave band (2 GHz–4 GHz). This frequency range matches the frequency range of modern communication networks such as those used for cell-phones, radar, satellite communications, and WiFi. The chaos generator circuit takes advantage of widely available inexpensive components. Chaotic frequency-modulated microwave signals have been shown to offer advantages such as low probability of detection or interception in radar systems,

^{a)}Electronic mail: lehiendao@gmail.com.

reduced interference with existing channels, and less susceptibility to noise or jamming.¹⁶

The remainder of the paper is organized as follows: Section II introduces the design of the system and a mathematical model based on a delay-differential equation derived from basic electronics principles. In Sec. III, the system implementation is discussed. We describe the characteristics of the components comprising the feedback loop and discuss how the nonlinearity, delay, and filter functions work together to produce chaotic behavior. The results of the numerical calculation along with experimental data are presented in Sec. IV, in which we show typical dynamical behaviors and the route to chaos of the system. Section V introduces a new Boolean time-delayed feedback system, obtained by replacing the sinusoidal nonlinearity with a binary function. The resulting system is shown to exhibit complex periodic orbits and self-similar characteristics in its bifurcation diagram.

II. SYSTEM DESIGN

In Fig. 1, we illustrate the experimental configuration of a time-delayed feedback loop used to produce chaotic microwave signals. The microwave signal is generated by a voltage-controlled oscillator (VCO), which produces a constant-amplitude microwave signal with a frequency that varies linearly with an applied tuning voltage. The output signal from the VCO can be described by the complex microwave signal

$$E(t) = \sqrt{2A}e^{j[\omega_0 t + \theta(t)]}, \tag{1}$$

where A is a constant that is proportional to the microwave power, ω_0 is the natural frequency of the VCO, and the phase $\theta(t)$ is related to the applied voltage $v(t)$ by

$$\frac{d\theta}{dt} = 2\pi\gamma v(t). \tag{2}$$

The factor γ is a property of the VCO that describes the tuning sensitivity, typically given in MHz/V.

The microwave signal is then split into two paths, one of which is delayed with respect to the other by an amount τ_d . The two signals are fed into a down-converting double-balanced

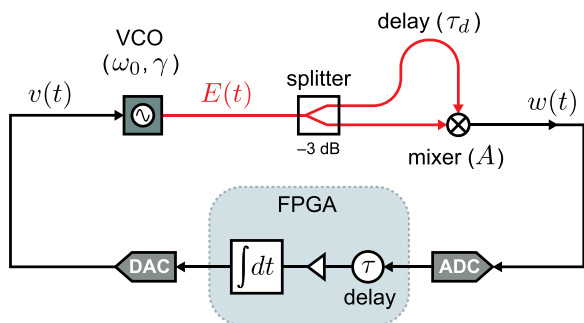


FIG. 1. Experimental system used to produce chaotic frequency-modulated microwave signals. The system uses a conventional microwave VCO with a homodyne microwave phase discriminator to produce a sinusoidal nonlinearity. The output is then fed back to the input through a time-delayed integrator which is implemented on a field-programmable gate array (FPGA).

mixer, thereby comprising a homodyne phase discriminator. The output w of an ideal balanced mixer with RF inputs E_1 and E_2 may be modeled as

$$w(t) = \text{Re}\{E_1(t)E_2^*(t)\}. \tag{3}$$

For the power splitter and delay line configuration shown in Fig. 1, the two mixer inputs are $E_1(t) = E(t)/\sqrt{2}$ and $E_2(t) = E(t - \tau_d)/\sqrt{2}$, which produces the output signal

$$w(t) = \frac{1}{2} \text{Re}\{E(t)E^*(t - \tau_d)\} = A \cos [\theta(t) - \theta(t - \tau_d) - \omega_0 \tau_d]. \tag{4}$$

If we further assume that $\theta(t)$ varies slowly on the timescale τ_d , Eq. (4) may be approximated by

$$w(t) = A \cos [\tau_d \dot{\theta}(t) - \omega_0 \tau_d] = A \cos [2\pi\gamma\tau_d v(t) - \omega_0 \tau_d]. \tag{5}$$

Finally, the output signal of the mixer is fed back to the VCO tuning input through a time delay τ and integrating filter, so that $v(t)$ and $w(t)$ are related by

$$v(t) = \frac{1}{T} \int_{-\infty}^t w(t' - \tau) dt', \tag{6}$$

where T is the integration time constant and τ is the feedback time delay, which is assumed to be much larger than the microwave delay τ_d . Differentiating Eq. (6) and making use of Eq. (5), we obtain a first-order delay differential equation for the tuning voltage $v(t)$

$$\frac{dv}{dt} = \frac{A}{T} \cos [2\pi\gamma\tau_d v(t - \tau) - \omega_0 \tau_d], \tag{7}$$

where the scale factor A is now understood to include the microwave power, mixer efficiency, splitter loss, and any baseband electrical gain in the feedback path.

We next define a normalized dimensionless voltage $x(t)$ as

$$x(t) \equiv 2\pi\gamma\tau_d v(t) - \omega_0 \tau_d - \frac{\pi}{2}, \tag{8}$$

which leads to the delay differential equation

$$\frac{dx}{dt} = -2\pi\gamma A \frac{\tau_d}{T} \sin[x(t - \tau)]. \tag{9}$$

Furthermore, by normalizing time in terms of the feedback delay τ , Eq. (9) simplifies to

$$\dot{x}(t) = -R \sin[x(t - 1)], \tag{10}$$

where the single dimensionless constant R is defined as

$$R \equiv \frac{2\pi\gamma A \tau_d \tau}{T}. \tag{11}$$

This equation was considered by Schanz *et al.*,²² who observed that phase-locked loops with a feedback delay can

also be described by this equation. It was later independently analyzed by Sprott, who pointed out that it is one of the simplest nonlinear delay differential equations that exhibits chaotic behavior.²³

III. SYSTEM IMPLEMENTATION

The VCO used in these experiments (Mini-Circuits SOS-3065-119+) had a center frequency of 3 GHz and a linear tuning coefficient of $\gamma = 175$ MHz/V. The microwave power produced by the oscillator was approximately 4 mW and was approximately independent of the input voltage $v(t)$. The microwave phase shift was implemented using a 2 m length semirigid coaxial cable, which produced a time delay of $\tau_d = 10$ ns. The double-balanced mixer (Mini-Circuits MCA 1-80LH+) had a downconversion gain of 5.9 dB, which produced a baseband voltage amplitude of $A = 0.2$ V. The baseband (IF) range of the mixer was from DC to 1250 MHz, and the tuning port of the VCO had a modulation bandwidth of 10 MHz. Together, these limit the maximum dynamical speed of the baseband signals $v(t)$ and $w(t)$ in a way that is not modeled by Eq. (10). We therefore adjusted the parameters of the experiment to ensure that the dynamical behavior was slow enough not to be band-limited by the mixer or VCO.

Fig. 2 plots the experimentally measured sinusoidal relationship between the tuning voltage v and the mixer output w , together with a best-fit sinusoid. From these measurements, one can determine the two constants $A = 0.2$ V and $(2\pi\gamma\tau_d)^{-1} = 0.5$ V. The deviation from a perfect sinusoidal nonlinearity is attributed to non-ideal voltage-dependent power from the VCO and the mixer non-ideality.

The time-delayed integral feedback was constructed using a digital delay line implemented on a field-programmable gate array (Altera Cyclone II FPGA). The mixer output $w(t)$ was digitized using an 8-bit analog to digital converter (National Semiconductor, ADC08200) at a sampling frequency $f_s = 15$ MHz. The digitized signal was delayed through a 600-stage shift register, to produce a time delay of $\tau = 40$ μ s, and the integration of Eq. (6) was approximated using a simple summing accumulator

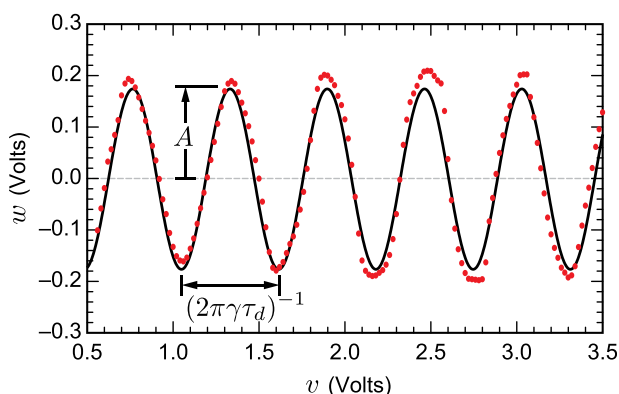


FIG. 2. Experimentally measured relationship between the input $v(t)$ and output $w(t)$ for the self-homodyne phase discriminator comprising a 10 ns microwave delay line and mixer. The solid curve indicates the best-fit sinusoidal function. From these measurements, one can determine the two constants $A = 0.2$ V and $(2\pi\gamma\tau_d)^{-1} = 0.5$ V, as shown.

$$v(t) = v(t - \Delta t) + \alpha w(t - N\Delta t), \quad (12)$$

where Δt is the sampling period. The discrete-time parameters N and α determine the feedback delay τ and integration time constant T , respectively, according to

$$\tau = N\Delta t, \quad T = \Delta t \frac{1}{\alpha}. \quad (13)$$

The resulting signal was converted back to an analog output voltage through a 10-bit digital to analog converter (TI DAC900) which was in turn applied to the input tuning port of the VCO. In the experiments reported, the feedback gain was manually adjusted or automatically swept by varying the constant α , which could be controlled by programming the FPGA.

The key experimental parameters of the system are summarized in Table I.

IV. DYNAMICAL BEHAVIOR

Because the nonlinear function is periodic in x , the solutions to Eq. (10) are easily seen to be translationally invariant up to an integer multiple of 2π . That is, if $x(t)$ is a solution, then $x(t) + 2\pi m$ is also a solution, for any integer m . For values of $R < 4.2$, we observe that the solution remains bounded within one cycle of the nonlinear function, with a peak-to-peak amplitude that is smaller than 2π . For larger values of R , the orbit is observed to hop between neighboring bound states, executing a kind of random walk behavior.²³ In practice, the voltage applied to the VCO is constrained to a limited range, and we therefore chose to restrict our attention to the regime in which $x(t)$ remains bounded. In the experiment, we observe the tuning voltage $v(t)$ on a digitizing oscilloscope. Additionally, we programmed the FPGA and DAC to also produce a second output channel that corresponds to the signal immediately prior to the integrator, which allows us to simultaneously observe $v(t)$ and $\dot{v}(t)$.

Fig. 3 compares characteristic phase portraits obtained from experimental measurements and numerical simulations, showing the variety of behaviors of the system. The simulated traces were calculated by numerically integrating Eq. (10), starting from random initial conditions, using a 5th order Dormand-Prince method with a constant step-size. The system was pre-iterated for a sufficiently long time to eliminate any transient behavior associated with non-physical initial conditions. In the

TABLE I. Summary of experimental parameters.

Parameter	Value
$f_s = 1/\Delta t$	15 Ms/s
N	600
τ	40 μ s
A	0.2 V
γ	175 MHz/V
τ_d	10 ns
$\omega_0/2\pi$	2.85 GHz
α	0.0067–0.0175
R	1.5–4.20

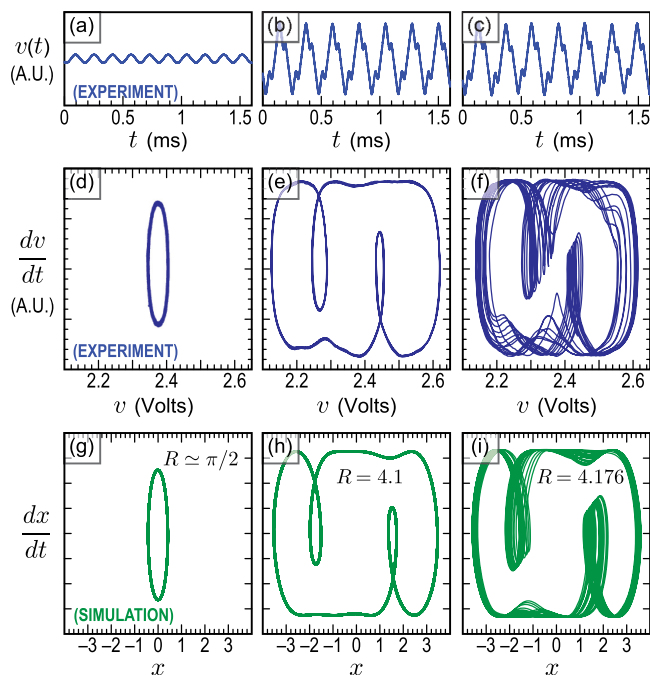


FIG. 3. Phase portraits of the system recorded experimentally (top) and simulated numerically (bottom) as the normalized feedback gain R is varied.

experiments, the feedback gain R was controlled by changing the integration proportionality constant α in Eq. (12), which could be adjusted to a precision of 40 bits by programming the FPGA. The output voltage from the DAC was offset in order to keep the system within the linear tuning range of the VCO.

Equation (10) admits a fixed point solution at $x=0$ that is stable whenever $R < \pi/2$. At $R = \pi/2$, the stable fixed point undergoes a Hopf bifurcation into a periodic state with a period of 4τ (6.25 KHz), as shown in Figs. 3(a), 3(d), and 3(g). The amplitude of $x(t)$ also increases with the feedback gain. At $R = 3.9$, the system makes a transition to a new periodic state, as shown in Figs. 3(b), 3(e), and 3(h), which exhibits a distinctly different point symmetry with respect to the origin. Above $R = 4.17$, system undergoes a period-doubling transition to chaos, resulting in the chaotic phase portraits shown in Figs. 3(c), 3(f), and 3(i). For the case of $R = 4.1758$, the Lyapunov spectrum was calculated numerically,^{24,25} which reveals a positive maximum Lyapunov exponent of $+5.316/\tau$ and a Kaplan-Yorke dimension of 2.15.

Fig. 4 presents both simulated and experimental bifurcation diagrams obtained by constructing a color histogram of characteristic time traces as the feedback gain R was smoothly increased from 1.5 to 4.2. For the experimental measurements, the proportionality between the integration factor α and the feedback gain R was inferred by empirically locating the value of α at which the first Hopf bifurcation occurs and associating this value with $R = \pi/2$. Apart from this scaling, there were no other adjustable parameters, and the theory exhibits good agreement with the experiment.

Fig. 5 plots the baseband spectrum of the tuning voltage $v(t)$ and the corresponding microwave spectrum produced by the VCO, for the case of $R = 4.176$, where the system is

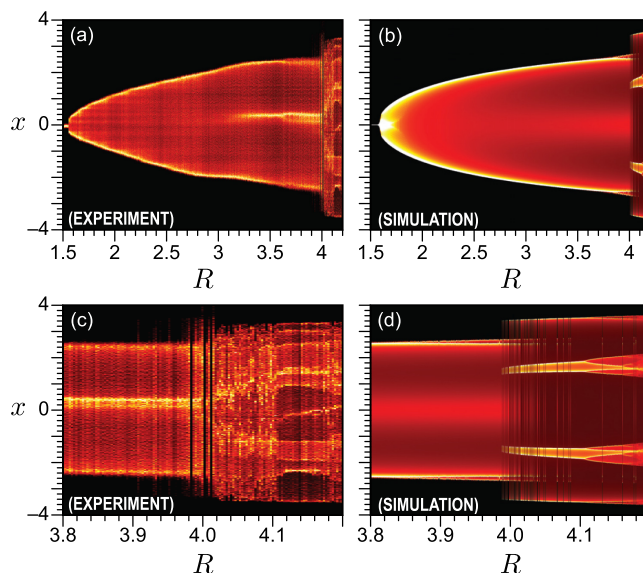


FIG. 4. Bifurcation diagrams for the system with $1.5 \leq R \leq 4.2$ were constructed using the Poincare section $dx/dt=0$. The experimental data were recorded using an 8-bit oscilloscope while the simulation results were obtained using MATLAB.

chaotic. Because of the large tuning sensitivity of the VCO (γ in Table I), the microwave signal occupies a much larger spectral bandwidth than the corresponding baseband signal. While in this demonstration, the bandwidth of $v(t)$ was approximately 10 kHz and could be scaled to approximately 10 MHz, at which point the dynamics would be constrained by the modulation bandwidth of the VCO.

V. BOOLEAN NONLINEARITY

An interesting and easily realized variation of this system is to replace the sinusoidal nonlinear function that relates v and w (cf. Fig. 2) with a Boolean relationship. In practice, this could be achieved by simply inserting a digital threshold device (comparator) following the mixer, thereby producing either a positive or negative output voltage of $w = \pm A$, depending on the sign of v . Experimentally, we achieve this by simply discarding all but the most significant (sign) bit during the analog-to-digital conversion of w .

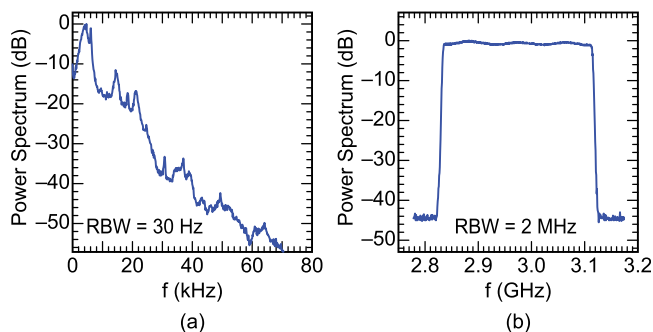


FIG. 5. (a) Measured baseband power spectrum of the signal entering the VCO, $v(t)$, and (b) corresponding microwave spectrum of the resulting frequency-modulated signal. Both measurements were taken with $R = 4.176$, which produces chaotic dynamics. The resolution bandwidth (RBW) was 30 Hz and 2 MHz for the baseband and microwave spectra, respectively, and both spectra were normalized relative to their maximum values.

Mathematically, this nonlinearity may be modeled by replacing Eq. (5) by the Boolean relationship

$$w(t) = A \operatorname{sgn}(\cos [2\pi\gamma\tau_d v(t) - \omega_0\tau_d]), \quad (14)$$

where sgn represents the algebraic sign function. In normalized time and amplitude units, the time-delayed dynamical equation becomes

$$\dot{x}(t) = -R \operatorname{sgn}(\sin[x(t-1)]) \quad (15)$$

$$= \begin{cases} +R, & \sin[x(t-1)] < 0 \\ -R, & \sin[x(t-1)] \geq 0 \end{cases} \quad (16)$$

where the single dimensionless constant R is defined as in Eq. (11).

Typical time traces along with time delay-embedding plots of $v(t)$ (or $x(t)$) are shown in Fig. 6. Unlike the earlier case, this system does not admit a fixed point solution for any value of R . Rather, the trajectories exhibit an alternating up-down sawtooth pattern that can be completely described by a sequence of switching times, i.e., the times at which the slope of $x(t)$ changes sign. These switching times can be calculated iteratively by locating the times at which $x(t-1)$ crosses a $m\pi$ threshold.

For values of $R < \pi$, the trajectories are symmetric triangular waves with a period of 4τ and a peak-to-peak amplitude of $2R$ centered about $x=0$, as shown in Figs. 6(a), 6(d), and 6(g). For $\pi < R < 4\pi/3$, the peak amplitude continues to grow in proportion to R , but the trajectories acquire secondary peaks on the rising and falling edge of the triangular wave, as shown in Figs. 6(b), 6(e), and 6(h). Above $R = 4\pi/3$, the behavior becomes more complicated, showing increasingly

longer-period trajectories that depend very sensitively on the feedback gain R , as in Figs. 6(c), 6(f), and 6(i). For all cases considered, the calculated dynamical behavior was observed to be periodic with an amplitude confined to the range $-R < x(t) < +R$, although the periodic orbits could contain as many as 54 segments, with periods approaching 60τ .

For $R > 3\pi/2$, the solutions no longer remain bounded, and $x(t)$ can instead exhibit a random-walk type behavior similar to what was observed for the sinusoidal case considered earlier. Even within this range, however, there exist isolated windows of R for which finite-amplitude solutions occur.

Fig. 7 presents a bifurcation diagram (experiment and simulation), showing the color-histogram of $x(t)$ as a function of the feedback gain R . Although the system is periodic for all points, the bifurcation diagram has a fractal characteristic in which any enlarged regions of the bifurcation appears self-similar to the original. This property is illustrated in Figs. 7(c) and 7(d), which show successive enlargements of the calculated bifurcation diagram.

While such a system can be classified as a continuous-time Boolean delay system, it does not fit the classic description of Ghil, for which the Boolean state depends only upon its prior value(s).²⁶ Rather, in this case, the Boolean slope $\dot{x}(t)$ depends on a prior value of $x(t-1)$. The system shares some features in common with earlier systems that exhibit a switching nonlinearity,²⁷ but it differs in that the dynamics are entirely characterized by the sequence of switching times.

The sawtooth waveforms generated by this system can have advantages for the frequency-modulated microwave system. The linear variation of the tuning frequency of the VCO produces a swept frequency signal with a linear chirp (positive or negative), which can simplify the signal processing for range-finding and Doppler velocity measurements.

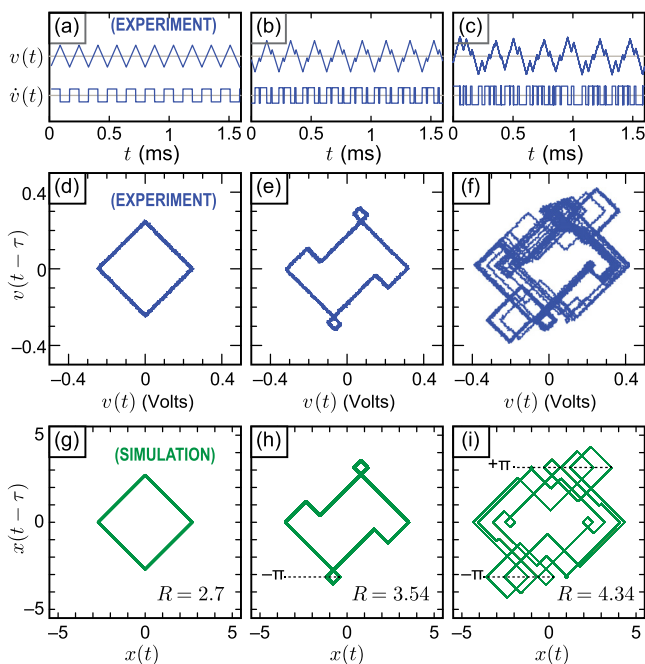


FIG. 6. Time traces and time delay embedding plots of the system using Boolean nonlinearity at different values of normalized feedback gain R .

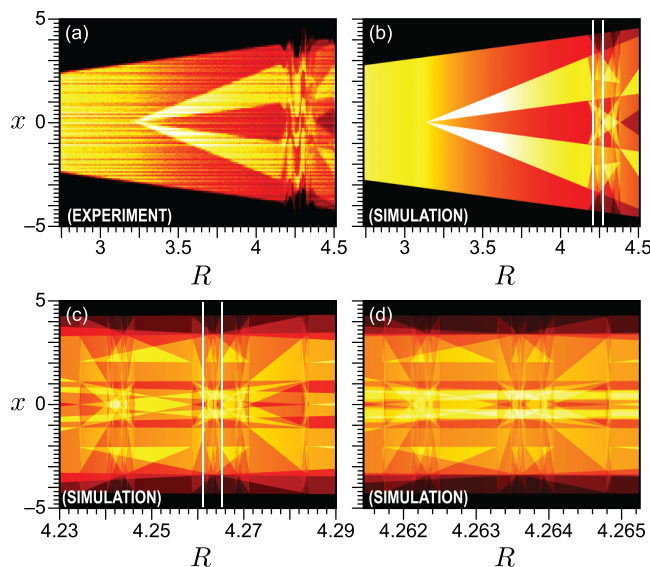


FIG. 7. Bifurcation diagram of the system utilizing the Boolean nonlinearity when R is varied from 2.75 to 4.5. (a) Experiment, (b)–(d) Simulation.

VI. CONCLUSION

We present the design and implementation of a microwave chaotic signal generator in the 2–4 GHz range that can generate deterministic, aperiodic frequency-modulated microwave signals. The system uses both microwave components and a field programmable gate array to implement the nonlinearity, the time delay, and the filtering functions. The system equation constitutes one of the simplest examples of a chaotic nonlinear chaotic delay differential equation. Numerical simulations of the system show good agreement with the observed behavior. By reprogramming the sinusoidal nonlinearity with a simple threshold-based nonlinearity, we realize a Boolean dynamical system that shows a range of periodicities and fractal characteristics, depending on the feedback strength or time delay. The system could find applications in chaotic radar or spread-spectrum communication systems.

ACKNOWLEDGMENTS

We thank Professor Rajarshi Roy for his valuable comments. This work was supported by DOD MURI Grant Nos. ONR N000140710734 and AFOSR FA95501010106.

- ¹G. Mazzini, R. Rovatti, and G. Setti, "Interference minimisation by auto-correlation shaping in asynchronous DS-CDMA systems: Chaos-based spreading is nearly optimal," *Electron. Lett.* **35**, 1054–1055 (1999).
- ²J. Deane and D. Hamill, "Improvement of power supply EMC by chaos," *Electron. Lett.* **32**, 1045 (1996).
- ³L. Fortuna, M. Frasca, and A. Rizzo, "Chaotic pulse position modulation to improve the efficiency of sonar sensors," *IEEE Trans. Instrum. Meas.* **52**, 1809–1814 (2003).
- ⁴J. Paul, S. Sivaprakasam, and K. A. Shore, "Dual-channel chaotic optical communications using external-cavity semiconductor lasers," *J. Opt. Soc. Am. B* **21**, 514–521 (2004).
- ⁵A. Argyris, D. Syvridis, L. Larger, V. Annovazzi-Lodi, P. Colet, I. Fischer, J. García-Ojalvo, C. R. Mirasso, L. Pesquera, and K. A. Shore, "Chaos-based communications at high bit rates using commercial fibre-optic links," *Nature* **438**, 343–346 (2005).
- ⁶K. Cuomo, A. Oppenheim, and S. Strogatz, "Synchronization of Lorenz-based chaotic circuits with applications to communications," *IEEE Trans. Circuits Syst., II: Analog Digital Signal Process.* **40**, 626–633 (1993).
- ⁷G. D. VanWiggeren and R. Roy, "Communication with chaotic lasers," *Science* **279**, 1198–1200 (1998).
- ⁸G. Bernstein and M. Lieberman, "Secure random number generation using chaotic circuits," *IEEE Trans. Circuits Syst.* **37**, 1157–1164 (1990).
- ⁹J. T. Gleeson, "Truly random number generator based on turbulent electro-convection," *Appl. Phys. Lett.* **81**, 1949 (2002).
- ¹⁰T. Stojanovski and L. Kocarev, "Chaos-based random number generators – Part I: Analysis," *IEEE Trans. Circuits Syst. I: Fundam. Theory Appl.* **48**, 281–288 (2001).
- ¹¹T. Stojanovski, J. Pihl, and L. Kocarev, "Chaos-based random number generators – Part II: Practical realization," *IEEE Trans. Circuits Syst. I: Fundam. Theory Appl.* **48**, 382–385 (2001).
- ¹²A. Uchida, K. Amano, M. Inoue, K. Hirano, S. Naito, H. Someya, I. Oowada, T. Kurashige, M. Shiki, S. Yoshimori, K. Yoshimura, and P. Davis, "Fast physical random bit generation with chaotic semiconductor lasers," *Nature Photon.* **2**, 728–732 (2008).
- ¹³K. Myneni, T. A. Barr, B. R. Reed, S. D. Pethel, and N. J. Corron, "High-precision ranging using chaotic laser pulse train," *Appl. Phys. Lett.* **74**, 1496–1498 (2001).
- ¹⁴B. Flores, E. Solis, and G. Thomas, "Assessment of chaos-based FM signals for range-Doppler imaging," *IEE Proc., Radar Sonar Navig.* **150**, 313–322 (2003).
- ¹⁵F.-Y. Lin and J.-M. Liu, "Chaotic radar using nonlinear laser dynamics," *IEEE J. Quantum Electron.* **40**, 815–820 (2004).
- ¹⁶T. L. Carroll, "Chaotic system for self-synchronizing Doppler measurement," *Chaos* **15**, 013109 (2005).
- ¹⁷K. Ikeda and K. Matsumoto, "High-dimensional chaotic behaviors in systems with time-delayed feedback," *Physica D* **29**, 223–235 (1987).
- ¹⁸J. N. Blakely, L. Illing, and D. J. Gauthier, "High-speed chaos in an optical feedback system with flexible timescales," *IEEE J. Quantum Electron.* **40**, 299–305 (2004).
- ¹⁹Y. C. Koumou, P. Colet, L. Larger, and N. Gastaud, "Chaotic breathers in delayed electro-optical systems," *Phys. Rev. Lett.* **95**, 203903 (2005).
- ²⁰A. B. Cohen, B. Ravoori, T. E. Murphy, and R. Roy, "Using synchronization for prediction of high-dimensional chaotic dynamics," *Phys. Rev. Lett.* **101**, 154102 (2008).
- ²¹V. S. Udaltsov, L. Larger, J. P. Goedgebuer, E. G. M. W. Lee, and W. T. Rhodes, "Band-pass chaotic dynamics of electronic oscillator operating with delayed nonlinear feedback," *IEEE Trans. Circuits Syst. I: Fundam. Theory Appl.* **49**, 1006–1009 (2002).
- ²²M. Schanz and A. Pelster, "Analytical and numerical investigations of the phase-locked loop with time delay," *Phys. Rev. E* **67**, 056205 (2003).
- ²³J. C. Sprott, "A simple chaotic delay differential equation," *Phys. Lett. A* **366**, 397–402 (2007).
- ²⁴J. D. Farmer, "Chaotic attractors of an infinite-dimensional dynamical system," *Physica D* **4**, 366–393 (1982).
- ²⁵H. F. vonBremen, F. E. Udwardia, and W. Proskurowski, "An efficient QR based method for the computation of Lyapunov exponents," *Physica D* **101**, 1–16 (1997).
- ²⁶M. Ghil, I. Zaliapin, and B. Coluzzi, "Boolean delay equations: A simple way of looking at complex system," *Physica D* **237**, 2967–2986 (2008).
- ²⁷N. J. Corron, J. N. Blakely, and M. T. Stahl, "A matched filter for chaos," *Chaos* **20**, 023123 (2010).